Chemosphere 93 (2013) 2514–2522

Contents lists available at ScienceDirect

Chemosphere

journal homepage: www.elsevier.com/locate/chemosphere

Nickel oxide nanoparticles exert cytotoxicity *via* oxidative stress and induce apoptotic response in human liver cells (HepG2)

Maqusood Ahamed [a,*], Daoud Ali [b], Hisham A. Alhadlaq [a,c], Mohd Javed Akhtar [a]

[a] King Abdullah Institute for Nanotechnology, King Saud University, Riyadh 11451, Saudi Arabia
[b] Cell and Molecular Laboratory, Department of Zoology, College of Science, King Saud University, Riyadh 11451, Saudi Arabia
[c] Department of Physics and Astronomy, College of Science, King Saud University, Riyadh 11451, Saudi Arabia

HIGHLIGHTS

- NiO NPs exerted cytotoxicity in human liver cells HepG2 in dose-dependent manner.
- NiO NPs induced ROS generation in dose-dependent manner.
- ROS scavenger vitamin C abolished almost fully the cytotoxic effect of NiO NPs.
- NiO NPs induced DNA damage, chromatin condensation and micronuclei induction.
- NiO NPs altered mRNA levels of apoptotic genes e.g. bax, bcl-2 and caspase-3.

ARTICLE INFO

Article history:
Received 5 May 2013
Received in revised form 29 August 2013
Accepted 10 September 2013
Available online 15 October 2013

Keywords:
NiO nanoparticles
Human health
Liver toxicity
ROS
Apoptosis

ABSTRACT

Increasing use of nickel oxide nanoparticles (NiO NPs) necessitates an improved understanding of their potential impact on human health. Previously, toxic effects of NiO NPs have been investigated, mainly on airway cells. However, information on effect of NiO NPs on human liver cells is largely lacking. In this study, we investigated the reactive oxygen species (ROS) mediated cytotoxicity and induction of apoptotic response in human liver cells (HepG2) due to NiO NPs exposure. Prepared NiO NPs were crystalline and spherical shaped with an average diameter of 44 nm. NiO NPs induced cytotoxicity (cell death) and ROS generation in HepG2 cells in dose-dependent manner. Further, ROS scavenger vitamin C reduced cell death drastically caused by NiO NPs exposure indicating that oxidative stress plays an important role in NiO NPs toxicity. Micronuclei induction, chromatin condensation and DNA damage in HepG2 cells treated with NiO NPs suggest that NiO NPs induced cell death via apoptotic pathway. Quantitative real-time PCR analysis showed that following the exposure of HepG2 cells to NiO NPs, the expression level of mRNA of apoptotic genes (bax and caspase-3) were up-regulated whereas the expression level of anti-apoptotic gene bcl-2 was down-regulated. Moreover, activity of caspase-3 enzyme was also higher in NiO NPs treated cells. To the best of our knowledge this is the first report demonstrating that NiO NPs caused cytotoxicity via ROS and induced apoptosis in HepG2 cells, which is likely to be mediated through bax/bcl-2 pathway. This work warrants careful assessment of Ni NPs before their commercial and industrial applications.

1. Introduction

Nanoparticles (NPs) have received tremendous international attention due to not only their wide-spread applications ranging from aerospace engineering and nano-electronics to environmental remediation and medical healthcare, but also their adverse effects to the environment and human health (Ahamed et al., 2008; Singh et al., 2009). NPs are the materials used in nanotechnology, which have at least one of their dimensions in the range of 1–100 nm. The crucial factors in NPs toxicity are size, chemical composition, shape and surface charge (Oberdoerster et al., 2005; Nel et al., 2006). Being smaller than cellular organelles and cells, it allows them to penetrate basic biological structures, which may in-turn disrupt their normal function (Buzae et al., 2007; Magaye and Zhao, 2012). Moreover, physicochemical properties of a NP cannot be simply predicted from the properties of a bulk particle with the same chemical composition (Magaye and Zhao, 2012). Studies have shown that NPs are more toxic than their bulk forms (Oberdorster, 2001; Zhang et al., 2010).

* Corresponding author. Address: King Abdullah Institute for Nanotechnology, King Saud University, P.O. Box 2454, Riyadh 11451, Saudi Arabia. Tel.: +966 4698781; fax: +966 4670664.
E-mail addresses: maqusood@gmail.com, mahamed@ksu.edu.sa (M. Ahamed).

0045-6535/$ - see front matter © 2013 Elsevier Ltd. All rights reserved.
http://dx.doi.org/10.1016/j.chemosphere.2013.09.047

Nickel oxide (NiO) NPs are utilized in various applications such as solar cells, catalysts, lithium-ion batteries, resistive random access memory, light-emitting diodes, electrochemical sensors and biosensors (Salimi et al., 2007; Rao and Sunandana, 2008). Increasing use of NiO NPs necessitates an improved understanding of their potential impact on the environment and human health. Recently, few reports have shown that NiO NPs exert toxicity to bacteria, microalgae and tomato (*Lycopersicon esculentum*) seedlings roots (Baek and An, 2011; Gong et al., 2011; Faisal et al., 2013). In mammalian systems, toxic effects of NiO NPs have been investigated, mainly on airway cells (Lu et al., 2009; Pietruska et al., 2011). NiO NPs induced significant lung toxicity and inflammation following intratracheal instillation in rats (Zhang et al., 1998; Ogami et al., 2009; Horie et al., 2011; Morimoto et al., 2011). On the other hand, no study, so far, have investigated possible mechanisms of NiO NPs toxicity in human liver, which is the primary organ of metabolism. Studies suggest that NPs get absorbed as they pass through the gastrointestinal tract and distributed different organs like liver via the circulatory system. Studies have shown that the NPs when orally administered to mice accumulate in liver and cause toxicity (Chen et al., 2007; Wang et al., 2008). NPs could be delivered into the gastrointestinal tract via accidental ingestion by those who work in the NPs manufacturing industry or NPs research laboratories or by drinking or eating water or food contaminated with NPs (Ahamed et al., 2010a; Sharma et al., 2012).

Intracellular generation of reactive oxygen species (ROS) is a crucial factor not only in apoptotic pathway, but also in DNA damage and many other cellular processes (Nel et al., 2006; Stone and Donaldson, 2006; Ahamed et al., 2010b). Therefore, present study was designed to investigate the underlying mechanisms of cytotoxicity and apoptosis induced by NiO NPs in human liver cells (HepG2). To achieve this goal, we determined the cell viability, ROS generation, micronuclei induction, chromosome condensation, DNA damage and expression of apoptotic genes in HepG2 cells exposed to NiO NPs. The HepG2 cell line is a classical hepatic model used to test particles/compounds that are potentially cytotoxic, genotoxic or affect hepatocyte functions (Zou et al., 2011; Ahmad et al., 2012; Piret et al., 2012).

2. Materials and methods

2.1. Chemicals and reagents

Dulbecco's modified eagle's medium (DMEM), hank's balanced salt solution (HBSS), fetal bovine serum (FBS), penicillin–streptomycin and trypsin were purchased from Invitrogen Co. (Carlsbad, CA, USA). The 3-(4,5-2-yl)-2,5-diphenyltetrazoliumbromide (MTT), 2,7-dichlorofluorescin diacetate (DCFH-DA) and vitamin C were obtained from Sigma–Aldrich (St. Louis, MO, USA). DNA Ladder assay kit was bought from Roche (Indianapolis, IN, USA). Caspase-3 enzyme assay kit was purchased from Bio-Vision Inc. (Milpitas, California, USA). All other chemicals used were of the highest purity available from commercial sources.

2.2. Synthesis of nickel oxide nanoparticles

NiO NPs were prepared by a solid-state reaction using nickel (II) acetate [$Ni(CH_3COO)_2{\cdot}4H_2O$] and sodium hydroxide (NaOH) as the raw materials and Tween 80 as a dispersant (Wang et al., 2005). In brief, $Ni(CH_3COO)_2{\cdot}4H_2O$ and NaOH were grinded with appropriate amount of Tween 80 in an agate mortar at room temperature for about half an hour. Then product was washed with distilled water, treated in an ultrasonic bath with absolute ethanol and centrifuged. After that samples were dried in desiccators at 80 °C for 4 h. A light green powder of NiO NPs was obtained which was sintered at 400 °C for 2 h.

2.3. Characterization of nickel oxide nanoparticles

Crystalline nature of NiO NPs was carried out by X-ray diffraction (XRD). The XRD pattern of NiO NPs was acquired at room temperature with the help of PANalytical X'Pert X-ray diffractometer equipped with a Ni filter using Cu Kα (λ = 1.54056 Å) radiations as an X-ray source. Shape and size of NiO NPs were determined by field emission transmission electron microscopy (FETEM, JEM-2100F, JEOL Inc., Japan) at an accelerating voltage of 200 kV as described in our previous publication (Ahamed et al., 2010). In brief, dry powder of Ni NPs was suspended in deionized water at a concentration of 1 mg mL^{-1}, and then sonicated using a sonicator bath at room temperature for 15 min at 40 W to form a homogeneous suspension. For size measurement, sonicated 1 mg mL^{-1} Ni NPs stock solution was then diluted to a 50–100 μg mL^{-1} working solutions. A drop of aqueous Ni NP suspension was placed onto a carbon-coated copper grid, air dried and observed with TEM.

The average hydrodynamic size and zeta potential of ZnO NPs in water and complete cell culture medium were determined by dynamic light scattering (DLS) (Nano-ZetaSizer-HT, Malvern Instruments, Malvern, UK) as described by Murdock et al. (2008). In brief, dry powder of Ni NPs was suspended in water and cell culture medium at a concentration of 100 μg mL^{-1} for 24 h. Then suspension of Ni NPs was sonicated using a sonicator bath at room temperature for 15 min at 40 W and the DLS experiments performed.

2.4. Cell culture and treatment of nickel oxide nanoparticles

HepG2 cells were obtained from American Type Culture Collection (ATCC) (Manassas, VA, USA). Cells were used between 10 and 20 passages. Cells were cultured in MEM medium supplemented with 10% FBS, 100 U mL^{-1} penicillin–streptomycin, 1 mM sodium pyruvate and 1.5 g L^{-1} sodium bicarbonate at 5% CO_2 and 37 °C. At 85% confluence, cells were harvested using 0.25% trypsin and were sub-cultured. Cells were allowed to attach the surface for 24 h prior to treatment. Dry powder of NiO NPs was suspended in cell culture medium at a concentration concentration of 1 mg mL^{-1} and diluted to appropriate concentrations (2–100 μg mL^{-1}). The dilutions of NiO NPs were then sonicated using a sonicator bath at room temperature for 15 min at 40 W to avoid NPs agglomeration prior to cell exposure. Under some conditions, HepG2 cells were pre-exposed for 1 h with 1.5 mM of vitamin C before 24 h co-exposure with or without NiO NPs. Cells not exposed to NiO NPs served as controls in each experiment.

2.5. Cell viability assay

Cell viability (MTT assay) was carried out following the procedure as described by Mossman (1983) with some modifications (Ahamed et al., 2011). The MTT assay assesses the mitochondrial function by measuring ability of viable cells to reduce MTT into blue formazan product. In brief, 1×10^4 cells/well were seeded in 96-well plates and exposed to different concentrations of NiO NPs (2–100 μg mL^{-1}) for 24 h. At the end of exposure, culture medium was removed from each well to avoid interference of NPs and replaced with new medium containing MTT solution in an amount equal to 10% of culture volume and incubated for 3 h at 37 °C until a purple-colored formazan product developed. The resulting formazan product was dissolved in acidified isopropanol. Further, the 96-well plate was centrifuged at 2300*g* for 5 min to settle down the remaining NPs. Then, a 100 μL supernatant was transferred to other fresh wells of a 96-well plate, and absorbance

was measured at 570 by using a microplate reader (Synergy-HT, BioTek, USA).

2.6. Assay of ROS generation

ROS generation was measured using 2,7-dichlorofluorescin diacetate (DCFH-DA) as described by Wang and Joseph (1999) with some modifications (Siddiqui et al., 2010). Generation of ROS was determined by two methods; fluorometric analysis and microscopic fluorescence imaging. For fluorometric analysis, cells (1×10^4 cells/well) were seeded in 96-well black-bottomed culture plates and allowed to adhere for 24 h in a CO_2 incubator at 37 °C. Next, HepG2 cells were exposed to different concentrations of NiO NPs (25–100 μg mL^{-1}) for 24 h. At the end of exposure, cells were washed twice with HBSS and then incubated in 1 mL of working solution of DCFH-DA at 37 °C for 30 min. Cells were lysed in alkaline solution and centrifuged at 2300*g* for 10 min. A 200 μL supernatant was transferred to a 96-well plate, and fluorescence was measured at 485 nm excitation and 520 nm emission using a microplate reader (Synergy-HT, BioTek). The values were expressed as a percent of fluorescence intensity relative to control wells. A parallel set of cells (5×10^4 cells/well) were analyzed for intracellular fluorescence using a fluorescence microscope (OLYMPUS CKX 41) by grabbing the images at 20× magnification.

2.7. Flow cytometry analysis for micronuclei induction

Micronuclei formation due NiO NPs exposure was examined using flow cytometer as described by Nusse et al. (1994). Briefly, exposed and control cells were washed with cold phosphate buffer saline. Further cell suspension was centrifuged for 5 min at 500*g* and supernatant was removed. Cell pellet was suspended in solution I (10 mM NaCl, 3.4 mM sodium citrate, 25 μg mL^{-1} propidium iodide, 0.01 mg RNase from bovine pancreas and 0.3 μL mL^{-1} triton-X). After 1 h at room temperature, an equal volume of solution II (78.1 mM citric acid, 40 μg mL^{-1} PI, and 0.25 M sucrose) was added. After 15 min, the suspension was filtered through a 53-mmnylon mesh and stored on ice until analyzed on flow cytometer (Becton–Dickinson LSR II, San Jose, CA, USA) using 'Cell Quest' 3.3 analysis software.

2.8. DAPI staining for chromosome condensation

Chromosome condensation in HepG2 cells due to NiO NPs exposure was observed by 4′,6-diamidino-2-phenylindole (DAPI) staining according to the method of Dhar-Mascareno et al. (2005). DAPI solution was used to stain the exposed cells in eight chamber slides and slides were incubated for 10 min in dark at 37 °C. Images of the nucleus were captured using a fluorescence microscope (OLYMPUS CKX 41).

2.9. DNA ladder assay

DNA ladder assay was performed in HepG2 cells exposed to 100 μg mL^{-1} NiO NPs for 24 h. At the end of exposure, DNA was extracted using a DNA Ladder Kit. The extracted DNA was then evaluated on a 1% agarose gel using ethidium bromide. DNA fragmentation pattern was observed in a gel documentation system.

2.10. Comet assay

Comet assay was performed as described by Singh et al. (1988) with some specific modifications (Ali et al., 2010). In brief, 70000 cells/well were seeded in a 12-well plate. After 24 h of seeding, cells were treated with different concentrations of NiO NPs (25–100 μg mL^{-1}) for 24 h. At the end of exposure, cells were trypsinized and re-suspended in DMEM supplemented with 10% FBS and cell suspension was centrifuged at 2300*g* for 5 min at 4 °C. The cell pellet was finally suspended in ice-chilled phosphate buffer saline for comet assay. Then, 15 μL of cell suspension (approximately 20000 cells) was mixed with 85 μL of low melting-point agarose (0.5%) and layered on one end of a frosted plain glass slide, pre-coated with a layer of 200 μL normal agarose (1%). Thereafter, it was covered with a third layer of 100 μL low melting-point agarose (0.5%). After solidification of the gel, the slides were immersed in a freshly prepared lysing solution (2.5 M NaCl, 100 mM Na_2EDTA and 10 mM Tris pH 10 with 10% DMSO and 1% Triton X-100) for overnight at 4 °C. The slides were then placed in a horizontal gel electrophoresis unit. Fresh cold alkaline electrophoresis buffer (300 mM NaOH, 1 mM Na_2EDTA and 0.2% DMSO, pH 13.5) was poured into the chamber and left for 20 min at 4 °C for DNA unwinding and conversion of alkali-labile sites to single-strand breaks. Electrophoresis was carried out using same solution at 4 °C for 20 min at 15 V. The slides were neutralized gently with 0.4 M tris buffer at pH 7.5 and stained with 75 μL ethidium bromide (20 μg mL^{-1}). The slides were stored at 4 °C in a humidified slide box until scoring. Slides were scored at a final magnification of 400× using an image analysis system (Biovis comet software) attached to a fluorescent microscope (Leica optiphase microscope) equipped with appropriate filters. An undamaged cell resembles an intact nucleus without a tail and a damaged cell has the appearance of a comet. The comet parameter used to measure DNA damage in the cells was % tail DNA (fraction of DNA in the tail). Images from 50 random cells (25 from each replicate slide) were analyzed for each experiment.

2.11. Quantitative real-time PCR analysis

Cells were cultured in 6-well plates and exposed to different concentrations (25–100 μg mL^{-1}) of NiO NPs for 24 h. At the end of exposure, total RNA was extracted by Qiagen RNeasy mini Kit (Valencia, CA, USA) according to the manufacturer's instructions. Concentration of the extracted RNA was determined using Nanodrop 8000 spectrophotometer (Thermo-Scientific, Wilmington, DE, USA), and the integrity of RNA was visualized on a 1% agarose gel using a gel documentation system (Universal Hood II, BioRad, Hercules, CA, USA). The first strand of cDNA was synthesized from 1 μg of total RNA by reverse transcriptase using M-MLV (Promega, Madison, WI, USA) and oligo (dT) primers (Promega) according to the manufacturer's protocol. Quantitative real-time PCR was performed by QuantiTect SYBR Green PCR kit (Qiagen) using an ABI PRISM 7900HT Sequence Detection System (Applied Biosystems, Foster City, CA, USA). Two microliters of template cDNA was added to the final volume of 20 μL of reaction mixture. Real-time PCR cycle parameters included 10 min at 95 °C followed by 40 cycles involving denaturation at 95 °C for 15 s, annealing at 60 °C for 20 s, and elongation at 72 °C for 20 s. The sequences of the specific sets of primer for bax, bcl-2, caspase-3 and β-actin used in this study are given in our previous publication (Ahamed et al., 2011). Expressions of selected genes were normalized to the β-actin gene, which was used as an internal housekeeping control.

2.12. Assay of caspase-3 enzyme

Activity of caspase-3 enzymes was measured in exposed and control cells using BioVision kit. This assay is based on the principle that activated caspases in apoptotic cells cleave the synthetic substrates to release free chromophore p-nitroanilide (pNA). The pNA generated after specific action of caspase-3 on tertrapeptide substrates was DEVD-pNA (Ahamed et al., 2011). The reaction mixture was consisted of 50 μL of cell extract protein (50 μg), 50 μL of 2× reaction buffer (containing 10 mM dithiothreitol) and 5 μL of

4 mM DEVD-pNA substrate in a total volume of 105 μL. The reaction mixture was incubated at 37 °C for 1 h and absorbance of the product was measured using a microplate reader (Synergy-HT, BioTek) at 405 nm according to manufacturer's protocol.

2.13. Protein estimation

The total protein content was measured by the Bradford Method (Bradford, 1976) using Bradford reagent (Sigma–Aldrich) and bovine serum albumin as the standard.

2.14. Statistical analysis

All the data represented in this study are means ± SD of three identical experiments made in three replicate. Statistical significance was determined by one-way analysis of variance (ANOVA) followed by Dunnett's multiple comparison test. Significance was ascribed at $p < 0.05$. All analyses were conducted using the Prism software package (GraphPad Software, Version 5.0).

3. Results

3.1. Characterization of nickel oxide nanoparticles

Sharp diffraction peaks shown in Fig. 1A indicates the crystalline nature of NiO NPs. No characteristic peak related to any impurities was observed. The existence of strong and sharp diffraction peaks at $2\theta = 37.42$, 43.63, 63.07, 75.39 and 79.66 corresponding to (111), (200), (220), (311) and (222) crystal plane, respectively (JCPDS Card No. 73-1523). The crystallite size has been estimated from XRD using the Scherer's equation (Patterson, 1939). The average crystallite size of NiO NPs calculated by Scherer's formula was around 44 nm. Fig. 1B shows the typical TEM image of NiO NPs. TEM average diameter was calculated from measuring over 100 particles in random fields of TEM view. The average TEM diameter of NiO NPs was also approximately 44 nm (size range 22–69 nm) supporting the XRD results.

The average hydrodynamic size of Ni NPs in water and cell culture media determined by DLS was 350 nm and 311 nm, respectively. Further, the zeta potential of Ni NPs in water and culture media was −13 mV and −18 mV, respectively.

3.2. Nickel oxide nanoparticles induced cytotoxicity

HepG2 cells were exposed to NiO NPs at the concentrations of 0, 2, 5, 10, 25, 50, 100 and 200 μg mL^{-1} for 24 h and cell viability was determined by MTT assay. We observed that NiO NPs up to concentration of 5 μg mL^{-1}, did not produce significant reduction in cell viability. As concentration of NPs increased to 10 μg mL^{-1} or above, reduction in cell viability was observed in dose-dependent manner. Cell viability decreased to 88%, 78%, 64%, 41% and 25% when cells exposed to NiO NPs at the concentrations of 10, 25, 50, 100 and 200 μg mL^{-1}, respectively (Fig. 2).

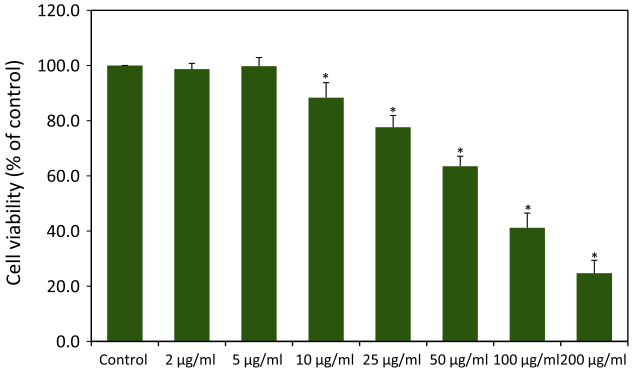

Fig. 2. NiO NPs induced cytotoxicity in HepG2 cells in dose-dependent manner. Data represented are mean ± SD of three identical experiments made in three replicate. *Statistically significant difference as compared to control ($p < 0.05$).

3.3. Nickel oxide nanoparticles induced intracellular ROS generation

Oxidative stress has been implicated as an explanation behind nanoparticles toxicity (Nel et al., 2006; Ahamed, 2013). Ability of NiO NPs to induce oxidative stress was assessed by measuring the ROS level in HepG2 cells. Both fluorescence microscopy (Fig. 3A) and quantitative data (Fig. 3B) revealed that NiO NPs (25–100 μg mL^{-1}) induce intracellular ROS generation in dose-dependent manner. Fig. 3A showed that fluorescence for ROS was detected in cells undergoing stress either lives or on the verge of death due to NiO NPs exposure. We also observed an inverse linear correlation between ROS and MTT (Fig. 3C).

3.4. Cytotoxicity of nickel oxide nanoparticles was mediated through ROS generation

In order to investigate whether ROS generation could play a role in cytotoxicity of NiO NPs, HepG2 cells were exposed to NiO NPs in presence of the vitamin C. Results showed that vitamin C prevented the ROS generation as well as abolished almost fully the cytotoxic effect of NiO NPs at all concentrations studied (25–100 μg mL^{-1}) (Fig. 4A and B).

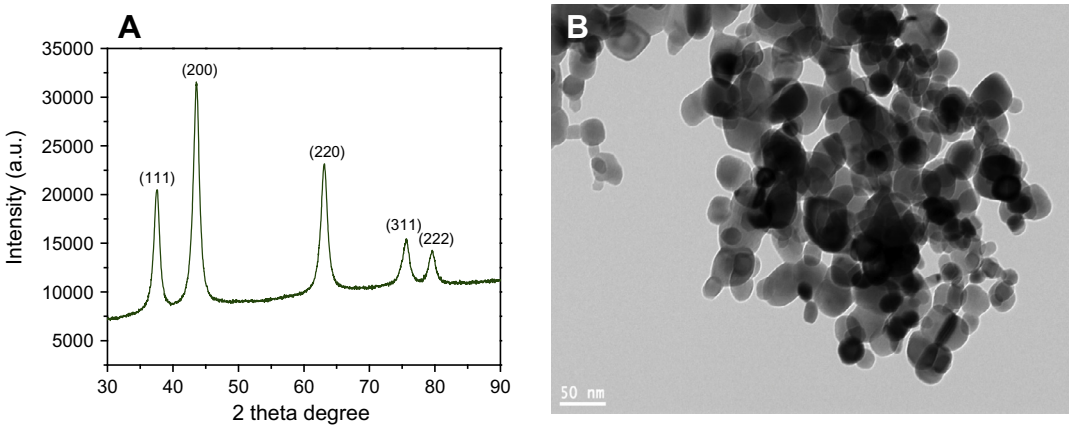

Fig. 1. Physico-chemical characterization of NiO NPs. (A) X-ray diffraction pattern of NiO NPs and (B) Transmission electron microscopy image of NiO NPs.

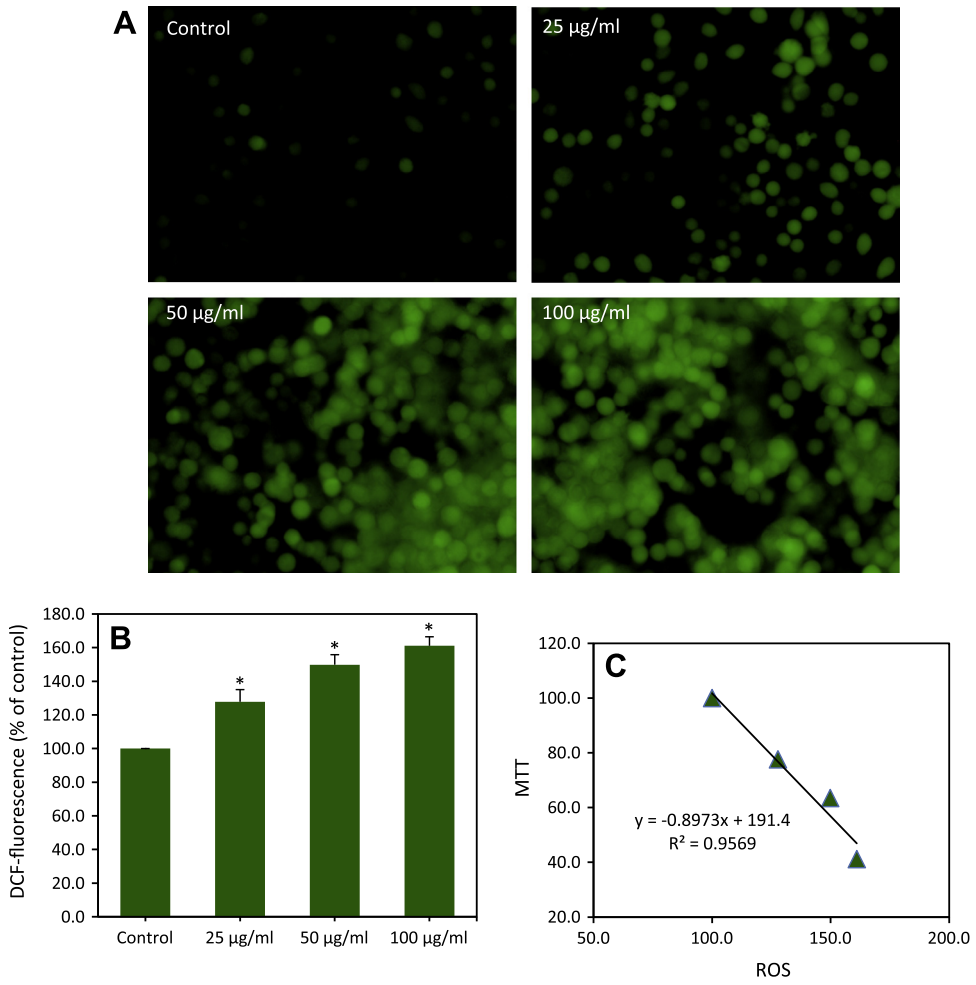

Fig. 3. NiO NPs induced ROS generation in HepG2 cells in dose-dependent manner. (A) Representative microphotographs showing NiO NPs induced ROS generation in HepG2 cells. Images were captured with a fluorescence microscope (OLYMPUS CKX 41). (B) Percentage change in ROS generation after 24 h exposure to different concentrations of NiO NPs in HepG2 cells. Data represented are mean ± SD of three identical experiments made in three replicate. *Statistically significant difference as compared to control ($p < 0.05$). (C) A significant negative correlation between ROS and MTT.

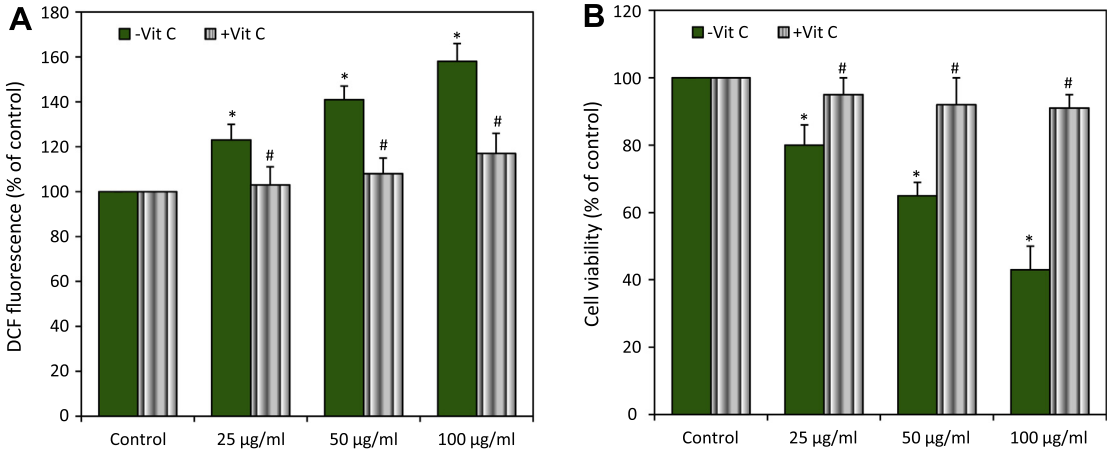

Fig. 4. Vitamin C prevented the ROS generation and preserved the viability (MTT assay) of HepG2 cells exposed to NiO NPs. (A) ROS level and (B) Cell viability. Data represented are mean ± SD of three identical experiments made in three replicate. *Statistically significant difference in ROS generation and cell viability reduction as compared to control ($p < 0.05$). #Significant inhibitory effect of vitamin C on ROS generation and cell viability reduction ($p < 0.05$).

3.5. Nickel oxide nanoparticles induced micronuclei induction, chromosome condensation and DNA fragmentation

Flow cytometry data revealed an increase in frequency of micronuclei in NiO NPs exposed cells (Fig. 5A and B). Chromatin condensation was evaluated by DAPI staining. When cells were treated with the above concentrations of NiO NPs for 24 h, chromatin condensation was observed in the treated group (Fig. 5C). We further analyzed the DNA profiles of the cells treated with NiO NPs. Results revealed that in control cells the DNA was not

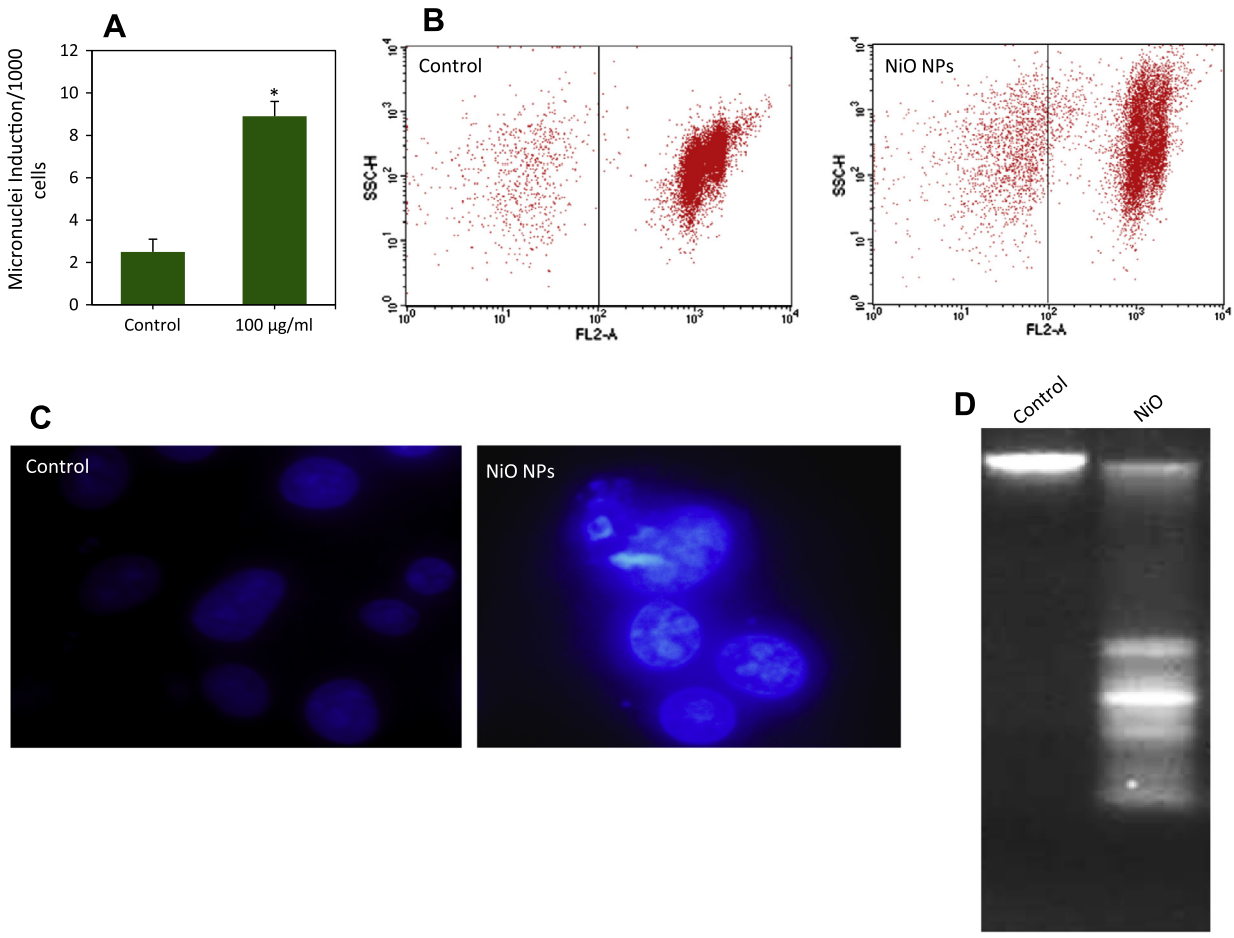

Fig. 5. NiO NPs induced mincronucei induction, chromosome condensation and DNA fragmentation in HepG2 cells. (A) Bar diagram of micronuclei formation in treated and control cells analyzed by flow cytometer. Data represented are mean ± SD of three identical experiments made in three replicate. *Significant difference as compared to the controls ($p < 0.05$). (B) Representative image of micronuclei induction of control and NiO NPs cells. (C) Representative photographs of DAPI staining for control and exposed cells. (D) DNA fragmentation.

fragmented, whereas the cells treated with NiO NPs had fragmented DNA (Fig. 5D). Micronuclei induction, chromatin condensation and DNA fragmentation in HepG2 cells suggest that NiO NPs induced cell death via apoptotic pathway.

3.6. Nickel oxide nanoparticles induced DNA damage

Comet assay, also called single cell gel electrophoresis (SCGE), determines a combination of single-strand breaks, double-strand breaks and alkaline labile sites (Olive and Durand, 1992; Yang et al., 2009). The DNA damage was measured as % tail DNA and olive tail moment in NiO NPs exposed cells and control cells. During electrophoresis, the cell DNA was observed to migrate more rapidly toward the anode at the highest concentration than the lowest concentration. The cells exposed to different concentrations of NiO NPs, exhibited higher DNA damage in cells than those of controls (Fig. 6A and B) ($p < 0.05$ for each). Fig 6C represents the photographs of DNA damage in HepG2 cells treated with NiO NPs.

3.7. Nickel oxide nanoparticles altered the expressions of mRNA level of apoptotic genes

Quantitative real-time PCR was utilized to analyze mRNA level of apoptotic genes (bax, bcl-2 and caspase-3) in HepG2 cells exposed to NiO NPs at the concentrations of 25, 50 and 100 µg mL^{-1} for 24 h. Results showed that NiO NPs altered the expressions of mRNA of these genes dose-dependently. The mRNA expression levels of apoptotic genes bax and caspase-3 were up-regulated while the expression level of anti-apoptotic gene bcl-2 was down-regulated in NiO NPs treated cells as compared to control (Fig. 7A) ($p < 0.05$ for each).

3.8. Nickel oxide nanoparticles induced caspase-3 enzyme activity

Activity of caspase-3 enzyme was also induced by NiO NPs supporting the real-time PCR results (Fig. 7B) ($p < 0.05$).

4. Discussion

Evidences of hazardous health effect of engineered NPs are rapidly increasing. As one of the toxic mechanisms of NPs, generation of ROS seems to be widely studied. NPs may alter ROS production and thereby may cause interference in biological antioxidant defense responses (Xia et al., 2008; Barillet et al., 2010). ROS in general cause DNA damage, including a multitude of oxidized base lesions, abasic sites, single and double-strand breaks; all of these can be cytotoxic and/or mutagenic (Diakowska et al., 2007; Paz-Elizur et al., 2008). However, studies on the exact mechanisms through which NPs generated ROS in cells are still underway. In this study, we evaluated the toxicity mechanisms of NiO NPs in human liver cell line (HepG2). Results showed that NiO NPs decreased cell viability dose-dependently. We hypothesized that

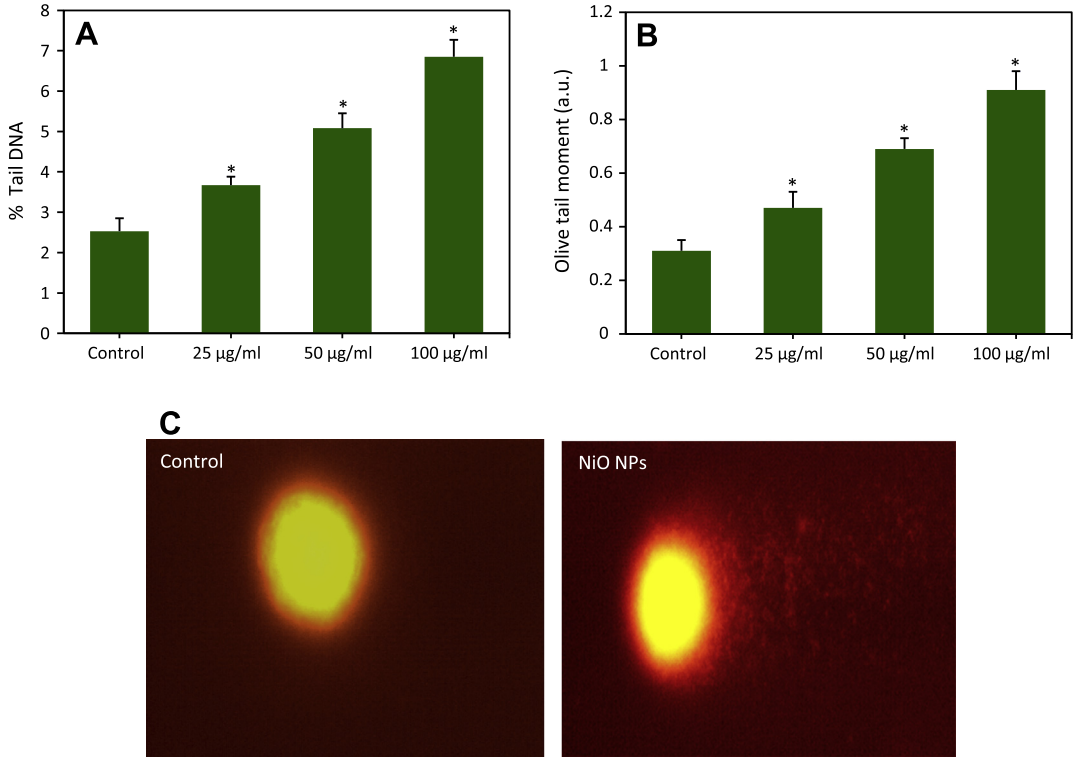

Fig. 6. NiO NPs induced DNA damage (comet assay) in HepG2 cells. (A) Percentage tail DNA and (B) olive tail moment (arbitrary unit). Data represented are mean ± SD of three identical experiments made in three replicate. *Significant difference as compared to the controls ($p < 0.05$ for each). (C) Representative photographs of DNA damage of control and treated cells.

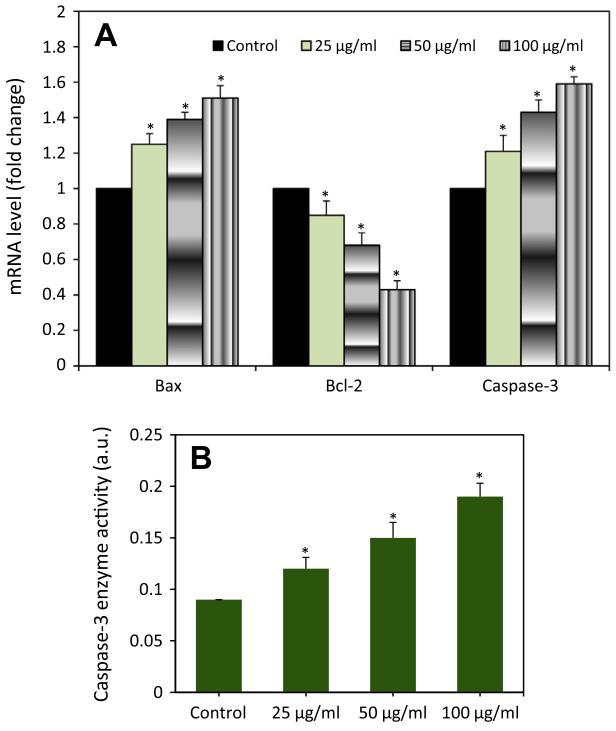

Fig. 7. NiO NPs induced apoptotic response in HepG2 cells. (A) Quantitative real-time PCR analysis of mRNA levels of bax, bcl-2 and casapase-3 genes in HepG2 cells exposed to different concentrations of NiO NPs. (B) NiO NPs induced the activity of caspase-3 enzyme in HepG2 cells. Data represented are mean ± SD of three identical experiments made in three replicate. *Statistically significant difference as compared to the controls ($p < 0.05$ for each).

NiO NPs induced cytotoxic response in HepG2 cells through ROS generation. Indeed, NiO NPs were shown to generate ROS in HepG2 cells as assayed by the 2,7-DCF probe oxidation measurement. Dose-dependent increase in ROS production was observed after 24 h exposure. These results confirm the oxidant potential of NiO NPs earlier described in other cell lines such as A549, HEp-2 and MCF-7 (Horie et al., 2011; Siddiqui et al., 2012). Moreover, ROS scavenger vitamin C reduced cell death drastically indicating that excessive ROS generation plays an important role in NiO NPs toxicity.

Apoptotic cell death is associated with a distinct set of biochemical and physical changes involving the cytoplasm, nucleus and plasma membrane. Early in apoptosis, cells round up, losing contact with their neighbors and shrink. In cytoplasm, endoplasmic reticulum dilates and cisternae swell to form vesicles and vacuoles. In nucleus, chromatin condenses and aggregates into dense compact masses (Lawen, 2003). In the present study, DAPI staining revealed that after treatment of NiO NPs, the cell nuclei were changed significantly, including the nuclear turned rippled or creased and nuclear condensation, suggesting that NiO NPs could influence the morphology of cell nuclei and further interference their functions. Micronuclei induction measurement is an established cytogenetic assay that can detect acentric fragments and lagging chromosomes induced by clastogens and aneugens (Heddle et al., 2011). The micronuclei induction measurement manually is usually conducted microscopically and is limited to two dimensions and, hence, some micronuclei are not counted due to a lack of visibility. The micronuclei induction measurement by flow cytometry, however, is a powerful tool that has capability of analyzing thousands of events rapidly in three dimensions leading to a reduction of false negatives errors. Progress has been made to automate the scoring of micronuclei by flow cytometry (Roman et al., 1998;

Smolewksi et al., 2001; Dertinger et al., 2002). Our results indicated that NiO NPs was able to cause a significant increase in micronuclei induction in HepG2 cells. In agreement with chromosome condensation and micronuclei induction results we further found that NiO NPs caused DNA fragmentation in HepG2 cells.

To confirm the above results we further used comet assay to examine DNA damage response of NiO NPs. This assay is able to detect DNA damage i.e. single strand breakage or other lesions, such as alkali-labile sites, DNA cross-links and incomplete excision repair events (Gedic et al., 1992; Tice et al., 2000). This technique has been widely used in the fields of genetic toxicology (Tice et al., 2000; Buschini et al., 2003). Investigators have been utilizing the comet assay to examine genotoxic potential of different types of nanoparticles (Ali et al., 2010; Shukla et al., 2011). Our results also demonstrated that NiO NPs significantly induce DNA damage as evident by % tail DNA and olive tail moment.

ROS can also oxidize proteins and lipids, leading to generation of highly toxic electrophilic species which can initiate inappropriate or altered cellular signal transduction pathways and contribute to toxicity (Halliwell et al., 1992). It has been proved that mitochondrial outer membrane proteins, which are regulated by the anti- and pro-apoptotic members of the bcl-2 family, and proteins released from mitochondria, lead to activation of caspases and subsequent cell death (Kuwana and Newmeyer, 2003). The bcl-2 and bax are two discrete members of bcl-2 family. The bcl-2 blocks cell death following various stimuli, demonstrating a death-sparing effect; however, over expression of bax has a pro-apoptotic effect and bax also counters the anti-apoptotic activity of bcl-2 (Chougule et al., 2011). The ratio of bax to bcl-2 expression represents a cell death switch, which determines the life or death of cells in response to an apoptotic stimulus; an increased bax/bcl-2 ratio decreases the cellular resistance to apoptotic stimuli, leading to increased apoptotic cell death (Bai and Meng, 2005; Gao and Wang, 2009). Caspases are activated during apoptosis in many cells and are known to play a vital role in both initiation and execution of apoptosis. It was reported that caspase-3 is essential for cellular DNA damage and apoptosis (Janicke et al., 1998). In this study, we found that the expressions of mRNA levels of apoptotic genes bax and caspase-3 were up-regulated, whereas expression of anti-apoptotic gene bcl-2 was down-regulated in HepG2 cells due to NiO NPs exposure. Activity of caspase-3 enzyme was also higher in NiO NPs treated HepG2 cells.

It has been reported that Ni ions released from the surface of Ni or NiO NPs when they were suspended in aqueous state e.g. water and cell culture media. However, we did not examine the degree of ionization of NiO NPs in aqueous suspension and their effects on HepG2 cells. Ispas et al. (2009) found that NiO NPs was not likely a result solely of particles' dissolution, as soluble Ni ions alone caused much less toxicity to zebrafish embryos than NiO NPs. However, another recent study found that Ni ions and NiO NPs were equally toxic to human lung epithelial cells followed by metallic Ni NPs, but not by metallic Ni microparticles (Pietruska et al., 2011). Therefore, toxicity due to dissolution of metallic Ni or NiO NPs to biological systems needs further investigations.

5. Conclusions

We have shown that NiO NPs exert cytotoxicity and oxidative stress to human liver (HepG2) cells in dose-dependent manner. ROS scavenger vitamin C reduced cell death considerably indicating that oxidative stress plays a crucial role in nanocrystalline NiO toxicity. Micronuclei induction, chromatin condensation and DNA damage in HepG2 cells suggest that NiO NPs induced cell death via apoptotic pathway. Furthermore, quantitative real-time PCR analysis displayed that mRNA levels of genes involved in the apoptosis were also altered by NiO NPs. Overall, our data suggesting that NiO NPs exert cytotoxicity via ROS and induce apoptosis in HepG2 cells, which is likely to be mediated through bax/bcl-2 pathway. Further studies are needed to investigate role of ROS in signaling pathways of apoptosis in response to exposure to NiO NPs at *in vivo* level.

Acknowledgments

This work was funded by King Abdulaziz City for Science and Technology (KACST), Riyadh, Saudi Arabia under the National Plan for Science and Technology (NPST) (Grant No.: 10-NAN1201-02).

References

Ahamed, M., 2013. Silica nanoparticles induced cytotoxicity, oxidative stress and apoptosis in A549 and A431 cells. Hum. Exp. Toxicol. 32, 186–195.
Ahamed, M., Karns, M., Goodson, M., Rowe, J., Hussain, S., Schlager, J., Hong, Y., 2008. DNA damage response to different surface chemistry of silver nanoparticles in mammalian cells. Toxicol. Appl. Pharmacol. 233, 404–410.
Ahamed, M., Posgai, R., Gorey, T.M., Nielson, M., Hussain, S.M., Rowe, J., 2010a. Silver nanoparticles induced heat shock protein 70, oxidative stress and apoptosis in *Drosophila melanogaster*. Toxicol. Appl. Pharmacol. 242, 263–269.
Ahamed, M., AlSalhi, M.S., Siddiqui, M.K.J., 2010b. Silver nanoparticle applications and human health. Clin. Chim. Acta 411, 1841–1848.
Ahamed, M., Akhtar, M.J., Siddiqui, M.A., Ahmad, J., Musarrat, J., Al-Khedhairy, A.A., Alrokayan, S.A., 2011. Oxidative stress mediated apoptosis induced by nickel ferrite nanoparticles in cultured A549 cells. Toxicology 283, 101–108.
Ahmad, J., Ahamed, M., Akhtar, M.J., Alrokayan, S.A., Siddiqui, M.A., Musarrat, J., Al-Khedhairy, A.A., 2012. Apoptosis induction by amorphous silica nanoparticles mediated through reactive oxygen species generation in human liver cell line HepG2. Toxicol. Appl. Pharmacol. 259, 160–168.
Ali, D., Ray, R.S., Hans, R.K., 2010. UVA-induced cytotoxicity and DNA damaging potential of benz (e) acephenanthrylene. Toxicol. Lett. 199, 193–200.
Baek, Y.-W., An, Y.-J., 2011. Microbial toxicity of metal oxide nanoparticles (CuO, NiO, ZnO, and Sb_2O_3) to *Escherichia coli*, *Bacillus subtilis*, and *Streptococcus aureus*. Sci. Total Environ. 409, 1603–1608.
Bai, J., Meng, Z., 2005. Effects of sulfur dioxide on apoptosis-related gene expressions in lungs from rats. Regul. Toxicol. Pharmacol. 43, 272–279.
Barillet, S., Jugan, M.L., Laye, M., Leconte, Y., Herlin-Boime, N., Reynaud, C., et al., 2010. In vitro evaluation of SiC nanoparticles impact on A549 pulmonary cells: cyto-, genotoxicity and oxidative stress. Toxicol. Lett. 198, 324–330.
Bradford, M.M., 1976. A rapid and sensitive method for the quantitation of microgram quantities of protein utilizing the principle of protein-dye binding. Anal. Biochem. 72, 248–254.
Buschini, A., Carboni, P., Martino, A., Poli, P., Rossi, C., 2003. Effects of temperature on baseline and genotoxicant-induced DNA damage in haemocytes of Dreissena polymorpha. Mutat. Res. 537, 81–92.
Buzae, C., Pacheco Blandino, I.I., Robbie, K., 2007. Nanomaterials and nanoparticles: sources and toxicity. Biointerphases 2 (4), MR17–MR172.
Chen, Z., Meng, H., Yuan, H., Xing, G., Chen, C., Zhao, F., et al., 2007. Identification of target organs of copper nanoparticles with ICPMS technique. J. Radioanal. Nucl. Chem. 272, 599–603.
Chougule, M., Patel, A.R., Sachdeva, P., Jackson, T., Singh, M., 2011. Anticancer activity of Noscapine, an opioid alkaloid in combination with cisplatin in human non-small cell lung cancer. Lung Cancer 71, 271–281.
Dertinger, S.D., Torous, D.K., Hall, N.E., Murante, F.G., Gleason, S.E., Miller, R.K., Tometsko, C.R., 2002. Enumeration of micronucleated CD71-positive human reticulocytes with a single-laser flow cytometer. Mutat. Res. 515, 3–14.
Dhar-Mascareno, M., Carcamo, J.M., Golde, D.W., 2005. Hypoxia-reoxygenation-induced mitochondrial damage and apoptosis in human endothelial cells are inhibited by vitamin C. Free Radical Biol. Med. 38, 1311–1322.
Diakowska, D., Lewandowski, A., Kopec, W., Diakowski, W., Chrzanowska, T., 2007. Oxidative DNA damage and total antioxidant status in serum of patients with esophageal squamous cell carcinoma. Hepatogastroenterology 78, 1701–1704.
Faisal, M., Saquib, Q., Alatar, A.A., Al-Khedhairy, A.A., Hegazy, A.K., Musarrat, J., 2013. Phytotoxic hazards of NiO-nanoparticles in tomato: a study on mechanism of cell death. J. Hazard. Mater. 250–251, 318–332.
Gao, C., Wang, A.Y., 2009. Significance of increased apoptosis and bax expression in human small intestinal adenocarcinoma. J. Histochem. Cytochem. 57, 1139–1148.
Gedic, C.M., Ewen, S.B., Collins, A.R., 1992. Single cell gel electrophoresis applied to analysis of UV-C damage and its repair in human cells. Int. J. Radiat. Biol. 62, 313–320.
Gong, N., Shao, K., Feng, W., Lin, Z., Liang, C., Sun, Y., 2011. Biotoxicity of nickel oxide nanoparticles and bio-remediation by microalgae Chlorella vulgaris. Chemosphere 83, 510–516.
Halliwell, B., Gutteridge, J.M., Cross, C.E., 1992. Free radicals, antioxidants, and human disease: where are we now? J. Lab. Clin. Med. 119, 598–620.
Heddle, J.A., Fenech, M., Hayashi, M., MacGregor, J.T., 2011. Reflections on the development of micronucleus assays. Mutagenesis 26, 3–10.

Horie, M., Fukui, H., Nishio, K., Endoh, S., Kato, H., Fujita, K., Miyauchi, A., Shichiri, M., Ishida, N., Kinugasa, S., Morimoto, Y., Niki, E., Yoshida, Y., Iwahashi, H., 2011. Evaluation of acute oxidative stress induced by NiO nanoparticles in vivo and in vitro. J. Occup. Health 53 (2), 64–74.
Ispas, C., Andreescu, D., Patel, A., Goia, D.V., Andreescu, S., Wallace, K.N., 2009. Toxicity and developmental defects of different sizes and shape nickel nanoparticles in zebrafish. Environ. Sci. Technol. 43, 6349–6356.
Janicke, R.U., Sprengart, M.L., Wati, M.R., Porter, A.G., 1998. Caspase-3 is required for DNA fragmentation and morphological changes associated with apoptosis. J. Biol. Chem. 273, 9357–9360.
Kuwana, T., Newmeyer, D.D., 2003. Bcl-2-family proteins and the role of mitochondria in apoptosis. Curr. Opin. Cell. Biol. 15, 691–699.
Lawen, A., 2003. Apoptosis-an introduction. BioEssays 25, 888–896.
Lu, S., Duffin, R., Poland, C., Daly, P., Murphy, F., Drost, E., MacNee, W., Stone, V., Donaldson, K., 2009. Efficacy of simple short-term in vitro assays for predicting the potential of metal oxide nanoparticles to cause pulmonary inflammation. Environ. Health Perspect. 117, 241–247.
Magaye, R., Zhao, J., 2012. Recent progress in studies of metallic nickel and nickel-based nanoparticles genotoxicity and carcinogenicity. Environ. Toxicol. Pharmacol. 34, 644–650.
Morimoto, Y., Hirohashi, M., Ogami, A., Oyabu, T., Myojo, T., Hashiba, M., Mizuquchi, Y., Kambara, T., Lee, B.W., Kuroda, E., Tanaka, I., 2011. Pulmonary toxicity following an intratracheal instillation of nickel oxide nanoparticle agglomerates. J. Occup. Health 53 (4), 293–295.
Mossman, T., 1983. Rapid colorimetric assay for cellular growth and survival: application to proliferation and cytotoxicity assays. J. Immunol. Methods 65, 55–63.
Murdock, R.C., Braydich-Stolle, L., Schrand, A.M., Schlager, J.J., Hussain, S.M., 2008. Characterization of nanomaterial dispersion in solution prior to in vitro exposure using dynamic light scattering technique. Toxicol. Sci. 101, 239–253.
Nel, A., Xia, T., Madler, L., Lin, N., 2006. Toxic potential of materials at the nano level. Science 311, 622–627.
Nusse, M., Beisker, W., Kramer, J., Miller, B.M., Schreiber, G.A., Viaggi, S., et al., 1994. Measurement of micronuclei by flow cytometry. In: Darzynkiewicz, Z., Robinson, J.P., Crissman, H.A. (Eds.), Methods in Cell Biology. Academic Press, San Diego, pp. 149–158.
Oberdoerster, G., Oberdoerster, E., Oberdoerster, J., 2005. Nanotoxicology: an emerging discipline evolving from studies of ultrafine particles. Environ. Health Perspect. 113, 823–839.
Oberdorster, G., 2001. Pulmonary effects of inhaled ultrafine particles. Int. Arch. Occup. Environ. Health 74 (1), 1–8.
Ogami, A., Morimoto, Y., Myojo, T., Oyabu, T., Murakami, M., Todoroki, M., Nishi, K., Kadoya, C., Yamamoto, M., Tanaka, I., 2009. Pathological features of different sizes of nickel oxide following intratracheal instillation in rats. Inhal. Toxicol. 21, 812–818.
Olive, P.L., Durand, R.E., 1992. Detection of hypoxic cells in a murine tumor with the use of the comet assay. J. Natl. Cancer Inst. 84, 707–711.
Patterson, A.L., 1939. The Scherrer formula for X-ray particle size determination. Phys. Rev. 56, 978–982.
Paz-Elizur, T., Sevilya, Z., Leitner-Dagan, Y., Elinger, D., Roisman, L.C., Livneh, Z., 2008. DNA repair of oxidative DNA damage in human carcinogenesis: potential application for cancer risk assessment and prevention. Cancer Lett. 266, 60–72.
Pietruska, J.R., Liu, X., Smith, A., McNeil, K., Weston, P., Zhitkovich, A., Hurt, R., Kane, A.B., 2011. Bioavailability, intracellular mobilization of nickel, and HIF-1 activation in human lung epithelial cells exposed to metallic nickel and nickel oxide nanoparticles. Toxicol. Sci. 124, 138–148.
Piret, J.P., Jacques, D., Audinot, J.N., Mejia, J., Boilan, E., Noël, F., Fransolet, M., Demazy, C., Lucas, S., Saout, C., Toussaint, O., 2012. Copper (II) oxide nanoparticles penetrate into HepG2 cells, exert cytotoxicity via oxidative stress and induce pro-inflammatory response. Nanoscale 4, 7168–7184.
Rao, K.V., Sunandana, C.S., 2008. Effect of fuel to oxidizer ratio on the structure, micro structure and EPR of combustion synthesized NiO nanoparticles. J. Nanosci. Nanotechnol. 8 (8), 4247–4253.
Roman, D., Locher, F., Suter, W., Cordier, A., Bobadilla, M., 1998. Evaluation of a new procedure for the flow cytometric analysis of in vitro, chemically induced micronuclei in V79 cells. Environ. Mol. Mutagen. 32, 387–396.
Salimi, A., Sharifi, E., Noorbakhsh, A., Soltanian, S., 2007. Direct electrochemistry and electrocatalytic activity of catalase immobilized onto electrodeposited nanoscale islands of nickel oxide. Biophys. Chem. 125, 540–548.
Sharma, V., Anderson, D., Dhawan, A., 2012. Zinc oxide nanoparticles induce oxidative DNA damage and ROS-triggered mitochondria mediated apoptosis in human liver cells (HepG2). Apoptosis 17, 852–870.
Shukla, R.K., Sharma, V., Pandey, A.K., Singh, S., Sultana, S., Dhawan, A., 2011. ROS-mediated genotoxicity induced by titanium dioxide nanoparticles in human epidermal cells. Toxicol. In Vitro 25, 231–241.
Siddiqui, M.A., Kashyap, M.P., Kumar, V., Al-Khedhairy, A.A., Musarrat, J., Pant, A.B., 2010. Protective potential of trans-resveratrol against 4-hydroxynonenal induced damage in PC12 cells. Toxicol. In Vitro 24, 1592–1598.
Siddiqui, M.A., Ahamed, M., Ahmad, J., Khan, M.A.M., Musarrat, J., Al-Khedhairy, A.A., Alrokayan, S.A., 2012. Nickel oxide nanoparticles induce cytotoxicity, oxidative stress and apoptosis in cultured human cells that is abrogated by the dietary antioxidant curcumin. Food Chem. Toxicol. 50, 641–647.
Singh, N.P., McCoy, M.T., Tice, R.R., Schneider, E.L., 1988. A simple technique for quantization of low levels of DNA damage in individual cells. Exp. Cell. Res. 175, 184–191.
Singh, N., Manshian, B., Jenkins, G.J., Griffiths, S.M., Williams, P.M., Maffeis, T.G., Wright, C.J., Doak, S.H., 2009. NanoGenotoxicology: the DNA damaging potential of engineered nanomaterials. Biomaterials 30, 3891–3914.
Smolewksi, P., Ruan, Q., Vellon, L., Darzynkiewicz, Z., 2001. Micronuclei assay by laser scanning cytometry. Cytometry 45, 19–26.
Stone, V., Donaldson, K., 2006. Nanotoxicology: signs of stress. Nat. Nanotech. 1, 23–24.
Tice, R.R., Agurell, E., Anderson, D., Burlinson, B., Hartmann, A., Kobayashi, H., et al., 2000. Single cell gel/comet assay: guidelines for in vitro/and in vivo genetic toxicology testing. Environ. Mol. Mutagen. 35, 206–221.
Wang, H., Joseph, J.A., 1999. Quantifying cellular oxidative stress by dichlorofluorescin assay using microplate reader. Free Radical Biol. Med. 27, 612–616.
Wang, Y., Zhu, J., Yang, X., Lu, L., Wang, X., 2005. Preparation of NiO nanoparticles and their catalytic activity in the thermal decomposition of ammonium perchlorate. Thermochim. Acta 437, 106–109.
Wang, B., Feng, W., Wang, M., Wang, T., Gu, T., Zhu, M., et al., 2008. Acute toxicological impact of nano- and submicro-scaled zinc oxide powder on healthy adult mice. J. Nanopart. Res. 10, 263–276.
Xia, T., Kovochich, M., Liong, M., Mädler, L., Gilbert, B., Shi, H., et al., 2008. Comparison of the mechanism of toxicity of zinc oxide and cerium oxide nanoparticles based on dissolution and oxidative stress properties. ACS Nano 2, 2121–2134.
Yang, H., Liu, C., Yang, D., Zhang, H., Xi, Z., 2009. Comparative study of cytotoxicity, oxidative stress and genotoxicity induced by four typical nanomaterials: the role of particle size, shape and composition. J. Appl. Toxicol. 29, 69–78.
Zhang, Q., Kusaka, Y., Zhu, X., Sato, K., Mo, Y., Donaldson, K., 1998. Differences in the extent of inflammation caused by intratracheal exposure to three ultrafine metals: role of free radicals. J. Toxicol. Environ. Health A 53, 423–438.
Zhang, X.D., Zhao, J., Bowman, L., Shi, X., Castranova, V., Ding, M., 2010. Tungsten carbide–cobalt particles activate Nrf2 and its downstream target genes in JB6 cells possibly by ROS generation. J. Environ. Pathol. Toxicol. Oncol. 29 (1), 31–40.
Zou, J., Chen, Q., Jin, X., Tang, S., Chen, K., Zhang, T., Xia, X., 2011. Olaquindox induces apoptosis through the mitochondrial pathway in HepG2 cells. Toxicology 285, 104–133.